Nanoscale

Accepted Manuscript

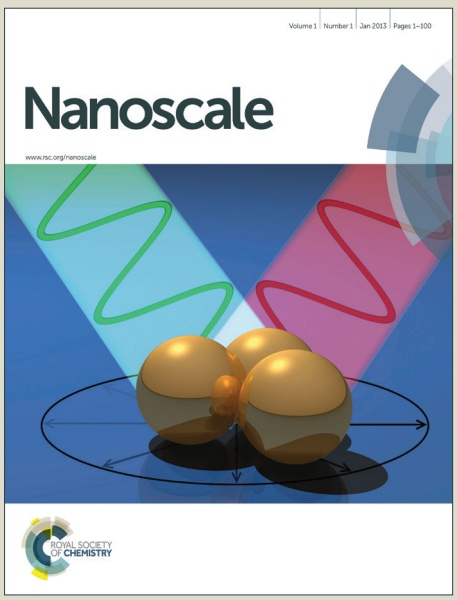

ROYAL SOCIETY OF CHEMISTRY

www.rsc.org/nanoscale

In-situ loading of well-dispersive silver nanoparticles on nanocrystalline magnesium oxide for real-time monitoring of catalytic reactions by surface enhancement Raman spectroscopy

Kaige Zhang, Gongke Li*, Yuling Hu*

School of Chemistry and Chemical Engineering, Sun Yat-sen University, Guangzhou, Guangdong 510275, P.R. China

* Corresponding author: G.K. Li, Y.L. Hu

Tel. : +86-20-84110922

Fax : +86-20-84115107

E. mail : cesgkl@mail.sysu.edu.cn

ceshyl@mail.sysu.edu.cn.

ABSTRACT

Surface-enhanced Raman spectroscopy (SERS) technique is of great importance for insight into the transient reaction intermediates and mechanistic pathways involved in heterogeneously catalyzed chemical reactions under actual reaction conditions, especially in water. Herein we demonstrate a facile method for in-situ synthesis of nanocrystalline magnesium oxide-Ag(0) (nano MgO-Ag(0)) hybrid nanomaterials with dispersive Ag nanoparticles (Ag NPs) on the surface of nanocrystalline magnesium oxide (nano MgO) via Sn^{2+} linkage and reduction. Benefit from the synergy effect of nano MgO and Ag NPs, the nano MgO-Ag(0) exhibited both excellent SERS and catalytic activities for the reduction of 4-nitrothiophenol in the presence of $NaBH_4$. The nano MgO-Ag(0) was used to real-time monitoring the catalytic reaction process of 4-nitrothiophenol to 4-aminothiophenol in aqueous medium by observing the SERS signals of the reactant, intermediate and final products. The intrinsic reaction kinetics and reaction mechanism of this reaction was also investigated. This SERS-based synergy technique provides a novel approach for quantitatively in-situ monitoring of catalytic chemical reaction processes.

Keywords: In-situ, nanocrystalline magnesium oxide-Ag(0), surface-enhanced Raman scattering, real-time monitoring, catalytic reaction.

Introduction:

Real-time monitoring of a heterogeneous reaction on a catalyst surface is fundamentally crucial for understanding the mechanisms and kinetics of the reaction. Carrying out these investigations under actual reaction conditions is preferred but remains challenging, especially for catalytic reactions that occur in water. Fourier transform infrared spectroscopy[1-3] and UV-vis[4] are candidate techniques for in-situ study of metal-catalyzed reactions. However, infrared spectroscopy in aqueous systems is complicated by the strong water absorption. UV-vis absorption spectroscopy provides only very limited chemical information. In contrast, surface enhanced Raman spectroscopy (SERS) which takes advantage of high sensitivity[5, 6], high chemical specificity[7] and surface selectivity[8], has opened up a new pathway for monitoring and controlling the catalytic reactions on metallic catalysts[9-15].

SERS applied in real-time monitoring of catalytic reactions requires developing appropriate bifunctional platform that is both plamonically and catalytically active. Bifunctional nanoparticles integrate two formerly distinct functionalities into a single entity with superior and some-times unprecedented properties. To date, only a limited number of bifunctional nanomaterials include Au and Pd alloy[9], Au and Pt alloy[10, 12, 14], Ag-doped titania nanoparticles[13], and Fe_3O_4@C@Au[15] were reported. But these bifunctional nanomaterials always need high requirement of preparation. Noble metal particles were also used to observe the catalytic reaction by SERS[16-18]. However, smaller noble metal particles aggregate very easily, resulting in a remarkable reduction in their catalytic and SERS activity.[19, 20] Considering these defects, our interest was to immobilize the noble metal nanoparticles on the surface of supports to prepare the bifunctional platform by a facile strategy.

The nano magnesium oxide (nano MgO) is a unique solid with highly ionic character, large specific surface area and crystal structure. These unique characteristics make them very

promising for diverse applications[21-23], for instance, as sorbents for surfactant molecules, supports for metal nanoparticles. To our knowledge, there are few reports about the construction of heterogeneous catalyst based on nano MgO support. Layek *et al*[22, 23] had successfully prepared gold nanoparticles supported on commercially available nano magnesium oxide, which were used as a heterogeneous catalyst. Nevertheless, the nanomaterials based on nano magnesium oxide support with both heterogeneous catalysis and SERS activity has never been reported.

In this work, we present a facile in-situ method to fabricate the nanocrystalline magnesium oxide-Ag(0) (nano MgO-Ag(0)) hybrid nanomaterials. The Sn^{2+} was linked to the surface of nano MgO through inorganic grafting. The Ag seed was formed by in-situ reducing $Ag(NH_3)_2^+$ by Sn^{2+}. Then high dispersive Ag NPs were subsequently generated on the surface of Ag seed. Under the synergy effect of nano MgO and Ag NPs, the nano MgO-Ag(0) exhibited excellent SERS and catalytic activities. Due to their dual functionalities, the nano MgO-Ag(0) was used to real-time monitoring the catalytic reaction process of 4-nitrothiophenol (4-NTP) to 4-aminothiophenol (4-ATP) in aqueous medium. The reaction path, mechanism and intrinsic reaction kinetics were also investigated.

Experimental

Regents and apparatus

Nanocrystalline magnesium oxide (nano MgO) was purchased from Beijing Nachen nano Co., Ltd (Beijing, China). Tin (II) chloride dehydrate ($SnCl_2 \cdot 2H_2O$) was purchased from Xilong Chemical Co., Ltd. (Guangzhou, China). Sodium borohydride ($NaBH_4$) (96%) and silver nitrate ($AgNO_3$) were purchased from Sinopharm Chemical Reagent Co., Ltd. (Shanghai, China). 4-NTP, 4-ATP, adenine, guanine, cytosine, thymine, uracil, methyl blue, malachite green, brilliant green, methyl green and rhodamine 6G were purchased from

Shanghai Jingchun Reagent Co., Ltd. (Shanghai, China). Hydrochloric acid (HCl), ammonium hydroxide ($NH_3 \cdot H_2O$), ethanol and formaldehyde (37%) were purchased by Damao Chemical Reagent Factory (Tianjin, China). All solvents and reagents were of analytical grade and directly used without further purification. Ultrapure water was used throughout the experiments.

Transmission electron microscopy (TEM) characterization was performed on a PHILIPS TECNAI 10 TEM instrument (Philips, Netherlands). X-ray diffractometry (XRD) was carried out using a RIGAKU diffractometer. X-ray photoelectron spectroscopy (XPS) experiments were performed on an ESCA LAB 250 XPS instrument. Infrared absorption spectra were conducted on a NICOLET AVATAR 330 Fourier transform infrared (FT-IR) spectrometer. BET experiments were performed on an ASAP 2020 Micropore Physisorption analyzer Standard. A battery-powered Raman spectrometer (model Inspector Raman, diode laser excitation wavelength λex¼785 nm) in the range 200-2200 cm^{-1} was used to provide the Raman spectra. This system consists of a liquid-N_2-cooled CCD detector (Model Spec-10:400B, Roper Scientific, Trenton, NJ) with a spectral resolution of 8 cm^{-1} and a data acquisition system (Photometrics, Tucson, AZ). Cary-100Conc UV-vis spectrophotometer (Varian, American) was employed.

In-situ loading of well-dispersive silver nanoparticles on the surface of nano MgO

10 mg of $SnCl_2 \cdot 2H_2O$ was dissolved in 10 mL of 10 mmol L^{-1} HCl solution. Then, 40 mg nano MgO was added into the above solution. nano MgO was calcined at 450 °C for four hours in air before use. After continuing stirring for 30 min at room temperature, the precipitate was recovered by centrifugation. Followed by washing with water three times, the precipitate was dispersive into 10 mL water. Thus, the activated nano MgO-Sn^{2+} was obtained. 10 mL of 0.01 mol L^{-1} $Ag(NH_3)_2^+$ solution was added to the activated solution and stirred for

about 30 min, then filtrated to obtain nano MgO containing Ag seeds (nano MgO-Ag_{seeds}). Subsequently, the nano MgO-Ag_{seeds} were redispersive into 10 mL of 0.01 mol L^{-1} $Ag(NH_3)_2^+$ solution and stirred. 500 μL of the mixture, which were composed of 0.4 mL of formaldehyde solution, 0.4 mL of deionized water and 9.2 mL of ethanol, was added into the above $Ag(NH_3)_2^+$ solution containing nano MgO-Ag_{seeds} drop by drop. The solution was stirred for another 30 min, then filtrated and washed with ultrapure water. Finally, it was dried in vacuum at 50 °C for one night to obtain nano MgO-Ag(0).

SERS experiments

For detection of dye molecules and nucleobases, 10 mg mL^{-1} nano MgO-Ag(0) solution was used. 3.0 μL nano MgO-Ag(0) was mixed with 3.0 μL analyte solution. Then the mixture was deposited onto a silicon substrate with dimensions of 0.5×0.5 cm^2. The silicon substrate was first washed by ultrasonication in acetone, ethanol, and water in turn. Then the substrate was treated in piranha solution (98%H_2SO_4/30%H_2O_2=3:1, v/v; CAUTION: piranha solution should be handled with great care) to clean the organic compounds and provide a hydroxylated surface. After being rinsed thoroughly with ultrapure water and dried by N_2 flow gas. A portable Raman spectrometer equipped with wavelength of 785 nm from an NIR diode laser and a power of 30 mW was used for SERS detection. The typical exposure time was 1 s with five accumulations. SERS were measured at room temperature with a portable Raman spectrometer.

Real-time monitoring of the catalytic hydrogenation of 4-NTP with SERS

The nano MgO-Ag(0) was used as bifunctional platform to real-time monitoring of catalytic hydrogenation of 4-NTP by SERS. Typically, 0.4 mL of 0.1 mmol L^{-1} 4-NTP solution, and 0.1 mL of 100 mmol L^{-1} of freshly prepared $NaBH_4$ aqueous solution were

added into glass tube under the N_2 balloon and stirred for 15 min respectively. The solution color turned to bright yellow rapidly due to the formation of 4-nitro-phenolate ion in alkaline condition. Subsequently, 0.2 mL of 10 mg mL^{-1} nano MgO-Ag(0) was added to start the reaction, and the intensity and Raman shift of peak were monitored by Raman spectroscopy equipped with 785 nm laser excitation. Successive SERS spectra were collected during the reaction until there were no noticeable changes between adjacent spectra.

Result and discussion

Preparation and characterization of nano MgO-Ag(0)

The nano MgO with certain physical and chemical properties enable it as a very suitable support for metal nanoparticles.[21-23] For example, there were a number of hydroxyl groups on the surface of nano MgO.[24, 25] Sn^{2+} chelate easily with hydroxyl groups through inorganic grafting. The standard reduction potential of the $Ag(NH_3)_2^+/Ag$ redox pair (0.373 V vs. SHE) is higher than that of Sn^{4+}/Sn^{2+} (0.151 V vs. SHE). Thus, the reduction of $Ag(NH_3)_2^+/Ag$ is easy. Herein we demonstrate a facile method for in-situ synthesis of nano MgO-Ag(0) hybrid nanomaterials with dispersive Ag NPs on the surface of nano MgO via Sn^{2+} linkage and reduction. The schematic illustration of the preparation was shown in **Fig. 1**. Firstly, the Sn^{2+} was linked onto the surface of nano MgO through inorganic grafting. Then, the linked Sn^{2+} acts as a reductant to in-situ reduce $Ag(NH_3)_2^+$ to Ag seeds (Ag_{seed}) and attach to the surface of the nano MgO. These Ag_{seed} are prerequisite for the subsequent steps leading to further particle growth. With formaldehyde added, the $Ag(NH_3)_2^+$ continues to be reduced and attached to the previously formed Ag_{seed}, leading to Ag NPs with controllable particle size. Here the Sn^{2+} acted as both "reducing reagent" and "positioning reagent", which anchor the

168 Ag_{seed} form at the location of the Sn^{2+}. Therefore, uniform Ag NPs could be directionally well
169 dispersive on the nano MgO substrate.

170 **Fig. 1**

171

172 XRD was also used to verify the formation of nano MgO-Ag(0). As can be seen from
173 **Fig. 2a**, the obvious diffraction peaks were observed at 38.115, 44.299, 64.443 and 77.397,
174 which can be indexed to the (111), (200), (220) and (311) planes correspond to face centred
175 cubic (FCC) crystalline lattice for metal silver (JCPDS No. 65-2871). The peaks
176 corresponding to (111) plane in Ag(0) nanoparticles has the highest intensity indicating that
177 this plane of nanocrystalline Ag(0) is the predominant crystal facet in nano MgO-Ag(0).
178 Richards and co-workers have reported that the (111) plane of nanostructured magnesium
179 oxide lattice possess the highest reactivity in chemical reactions.[26] The peaks that are indexed
180 as (001), (101), (102), (110), (111), (103) and (201) planes (given in parentheses, **Fig. 2a and**
181 **2b**) show the presence of hydrated hexagonal crystalline phase (JCPDS No. 07-0239) in nano
182 MgO-Ag(0) and pristine nano MgO Support. The peaks **(Fig. 2b)** corresponding to the planes
183 (111), (200), (220) and (222) show the presence of cubic crystalline phases as well (JCPDS
184 No. 75-0447) in pristine nano MgO lattice. The presence of mixed crystalline phases in nano
185 MgO is in accordance with the reports by Klabunde and co-workers[27].

186 **Fig. 2**

187

188 The morphology and structure of nano MgO and nano MgO-Ag(0) were examined by
189 TEM (**Fig. 3A**). The TEM of nano MgO-Ag(0) clearly showed good dispersion of spherical
190 Ag(0) on the surface of nano MgO support. The Ag NPs were remarkably well-dispersive,
191 and no aggregation was observed. The mean diameter of 101 Ag NPs in this TEM area is
192 9.97±1.95 nm. Selected area electron diffraction (SAED) image in the **Fig. 3B** indicated that

Ag NPs was polycrystalline structure. Furthermore, the presence of Ag element in the hybrid nanomaterials was confirmed by the energy-dispersive X-ray spectrum (EDS), as shown in **SI Fig. 1**.

Fig. 3

The FT-IR of the nano MgO support as well as the nano MgO-Ag(0) have also been investigated (**SI Fig. 2A**). The presence of weak-bonded -OH groups of nano MgO at 3698 cm^{-1} indicated that -OH groups existed in the nano MgO. The presence of non-bonded -OH groups at 3640 cm^{-1} indicated that the surface of nano MgO-Ag(0) became entirely hydroxylated during the preparation. This is consistent with the reactive profile of nano MgO in water[27].

UV-vis absorption spectra of aqueous dispersion of nano MgO and nano MgO-Ag(0) were shown in **SI Fig. 2B**. After decoration with Ag NPs on the surface of nano MgO, there was evidently a new peak at about 410 nm. This was the characteristic peak of Ag NPs due to the surface plasmon absorption, which implied successful formation of Ag NPs on the surface of nano MgO.

Furthermore, the presence of Ag element in the hybrids was confirmed further by XPS. As shown in **Fig. 4A**, the XPS revealed that nano MgO-Ag(0) consisted of the elements of Mg, O and Ag. The signals of Mg and O originated from nano MgO. The presence of Ag element in nano MgO-Ag(0) confirmed the successful reduction of $Ag(NH_3)_2^+$ on the surface of nano MgO. On the other hand, the Ag 3d spectrum for nano MgO-Ag(0) can be detected and the binding energy of Ag $3d_{5/2}$ and Ag $3d_{3/2}$ electrons for Ag element are identified to be 367.9 eV and 373.9 eV, respectively **(Fig. 4B)**.

Fig. 4

The BET specific surface area for the calcined nano MgO and nano MgO-Ag (0) was determined to be 467 and 140 m^2 g^{-1}, respectively. A relative high surface area of nano MgO support also facilitates the exposure of larger numbers of hydroxyl groups for further grafting, as well as providing more catalytically active metal at the same time.

SERS property

To investigate the SERS activity of the nano MgO-Ag(0), some dye molecules and nucleobases were used as SERS probes. The SERS spectra of methyl blue, malachite green, brilliant green, methyl green and rhodamine 6G were shown in **Fig. 5A**. The SERS spectra of several nucleobases were plotted in **Fig. 5B**. The SERS spectra of different dyes or nucleobases were significantly and easily discerned. Therefore, nano MgO-Ag(0) can be used as SERS active substrate for dye molecules' or nucleobases' identification and quantification. The enhancement factor of the nano MgO-Ag(0) as active substrate was 1.0×10^5-2.0×10^6 using dye molecules and nucleobases as the SERS probe molecule. These results indicated that the prepared nano MgO-Ag(0) are suitable as active substrate for SERS measurements.

Fig. 5

The uniformity and reproducibility of nano MgO-Ag(0) were also evaluated by SERS using 4-ATP as the probe molecules. We checked the reproducibility of the SERS measurement by recording spectra from the 40 randomly selected places on the same batch and taking SERS spectra with 30 different batches of the samples. The relative stand deviations of intensity at 1079 cm^{-1} Raman shift were 12.1% and 15.9% respectively (**Fig. 6**), which indicated that the nano MgO-Ag(0) as SERS substrate had high uniformity and good reproducibility. These results suggested that Ag NPs on the surface of nano MgO support was uniform and dispersive.

Fig. 6

Real-time monitoring of the catalytic hydrogenation of 4-NTP with SERS

Process of catalytic hydrogenation of 4-NTP

The plamonically and catalytically active properties of nano MgO-Ag(0) make it useful for real-time monitoring catalytic reaction by SERS. Here, we chose the nano MgO-Ag(0) as bifunctional platform for monitoring the catalytic hydrogenation of 4-NTP with an excess amount of $NaBH_4$ in colloidal suspension by SERS (inset of **Fig. 7**). Specifically, 4-NTP molecules firstly formed a monomolecular layer on the surface of nano MgO-Ag(0), where they were in-situ reduced to 4-ATP molecules by nano MgO-Ag(0) in the presence of $NaBH_4$. For starting the catalytic reaction, some volumes of 100 mmol L^{-1} $NaBH_4$ solution were added. The corresponding SERS spectra were recorded directly after the addition of different volumes. The SERS spectrum of the 4-NTP monolayer exhibited characteristic bands at 1076, 1347, and 1573 cm^{-1} that were assigned to C-S stretching, O-N-O stretching, and the phenyl-ring mode, respectively[18]. New Raman vibrational bands of an intermediate were observed upon addition of $NaBH_4$, which can be assigned to peaks of 4,4′-dimercapto-azobenzene (4,4′-DMAB). The three characteristic peaks at 1143, 1389 and 1432 cm^{-1} were due to C-N symmetric stretching, N=N stretching, and C-H in-plane bending modes, respectively.[28, 29] For large volume of $NaBH_4$, only additional bands of a third species were observed. These bands can be assigned to the corresponding aniline derivate RNH_2, in this case 4-ATP, which is the final reaction product for the reduction of 4-NTP by $NaBH_4$.

Fig. 7

Owing to the high SERS activity, the evolution of 4-NTP to 4-ATP with nano MgO-Ag(0) was explicitly reflected in a series of in-situ Raman spectra collected during the reaction process with the different reaction time. Process of reaction can be clearly observed by detecting spectra from the individual contributions of the involved molecular species, in this case the educt ($R\text{-}NO_2$), intermediate (R-N=N-R), and final product ($R\text{-}NH_2$). As shown in **Fig. 8**, the intensity of 4-NTP associated bands decreased with the conversion of 4-ATP at 1595 cm^{-1} emerged. New vibrational Raman bands of an intermediate were observed with the reaction time increasing, which can be assigned to 4,4′-DMAB. The three characteristic peaks were at 1143, 1389 and 1432 cm^{-1}, respectively.[28, 29] With further increase of the reaction time, the concentration of 4,4′-DMAB initially increased and then finally decreased. For enough long reaction time, only additional bands of a third species were observed. These bands can be assigned to final reaction product (4-ATP).

Fig. 8

To explore the synergy effect of nano MgO and Ag NPs for the monitoring of the catalytic hydrogenation of 4-NTP by SERS, the catalytical and SERS ability of the equal amount of pure nano MgO, Ag NPs and nano MgO-Ag(0) were studied. When nano MgO was used, **Fig. 9a-b** and **SI Fig. 3** showed that there were no Raman signals and obviously change of the UV-vis spectra. The result indicated that nano MgO has no Raman and catalytical activity. When Ag NPs was used, the characteristic peaks at 1143, 1389 and 1432 cm^{-1}, which can be assigned to 4,4′-DMAB, were obviously observed (**Fig. 9e-f**).[28, 29] The 4,4′-DMAB may be the surface-catalyzed dimerization of 4-NTP or the intermediate of the catalytic reaction.[30] The result of **Fig. 9e-f** indicated that Ag NPs has relatively lower catalytic activity for the catalytic reaction in this case. When nano MgO-Ag(0) was used, **Fig. 9c** showed the characteristic peak of 4-NTP, which is the reactant for the catalytic reaction. **Fig.**

9d showed the characteristic peak of 4-ATP, which is the final reaction product for the catalytic reaction. Fig. 9c-d indicated that nano MgO-Ag(0) has both stronger Raman and catalytical active. All above results confirmed that nano MgO played an important role in improving the catalytic and SERS activity of Ag NPs. On the one hand, nano MgO was used as support to immobilize the mono-dispersive Ag NPs, which was very important to prevent the aggregation of Ag NPs for use and storage. On the other hand, a relatively high surface area of nano MgO support also facilitates the exposure of comparatively larger numbers of active sites to adsorb 4-NTP to the surface of Ag NPs.

Fig. 9

Kinetics of catalytic hydrogenation of 4-NTP

The subsequent reduction of 4-NTP by the $NaBH_4$ should be a kinetically relevant step. Hence, the reaction kinetics can be quantified from the intensity evolution of the SERS bands of 4-NTP, which corresponds to its concentration variation. Here, the 1347 cm^{-1} was used for quantification. Since excess $NaBH_4$ was present in the reaction solution and remained constant during the reaction, the reaction could be considered pseudo-first-order with respect to 4-NTP. The pseudo-first-order reaction rate constant k can be determined by eq. (1).

$$k\,t = \ln (C_0/C_t) \qquad (1)$$

Here, C_0 and C_t are the concentration of reactant at the beginning and at time t, respectively. The relationship between SERS intensity and probe concentration can be determined by eq. (2).

$$I_{SERS} = k_1\,c \qquad (2)$$

Here, c is the concentration of the molecular probe and k_1 is constant for a substance. Thus, eq. (3) can be obtained from eq. (1) and (2).

$$k\,t = \ln([\text{4-NTP}]_0/[\text{4-NTP}]_t) = \ln([I_{1347}]_0/[I_{1347}]_t) \quad (3)$$

Here, [4-NTP] is the concentration of 4-NTP, and I_{1347} is the intensities of the bands at 1347 cm^{-1}. The logarithm of the ratio of the intensities at the beginning and at the time point t is plotted in **Fig. 10**. The catalytic reaction rate constant *k* was calculated to be 0.0095 s^{-1} at room temperature, which was higher than that reported for the same catalytic reaction using catalysts based on Au or Ag nanoparticles with varying morphologies and sizes.[15, 31, 32]

Fig. 10

The reusability studies of the nano MgO-Ag(0) catalyst was also carried out. After the reaction, the solid catalyst was separated by centrifugation. The catalyst was then washed with distilled water followed by ethanol and dried in N_2 balloon. After the three cycles, there was a gradual decrease in *k* with every reaction cycle **(SI Fig. 4)**. Primarily it may be assigned to the gradual loss in weight of the catalyst during recycling. To confirm these, the used catalyst (after different cycles) was examined by TEM. The TEM image of used nano MgO-Ag(0) catalyst **(SI Fig. 5)** showed no detach of the Ag NPs from supports and no agglomeration of the particles even after three reaction cycles. So the gradual decrease in *k* for the conversion of 4-NTP with every reaction cycle may be largely attributed to the loss in catalyst during recycling.

Probable reaction mechanism of catalytic hydrogenation of 4-NTP

Now there are two probable routes for the reduction of 4-NTP to 4-ATP based on the electrochemical model as presented by Haber[33] **(SI Fig. 6)**. In this reaction scheme, two different routes are proposed. In the direct route, the aromatic nitro compound is reduced to the nitroso compound and then further to the corresponding hydroxylamine in two very fast consecutive steps. Finally, the hydroxylamine is reduced to the aniline derivative in the

slowest reaction step (direct route, left pathway in **SI Fig. 6**). The second route proposed involved the condensation of nitroso compound with hydroxylamine to give the azoxy compound, which is reduced in a series of consecutive steps to the azo, hydrazo, and aniline compounds (condensation route, right pathway in **SI Fig. 6**).

As shown in **Fig. 8**, the reaction process of catalytic hydrogenation of 4-NTP was real-time monitored by SERS. The presence of 4,4′-DMAB (azo compounds) in the reaction mixture signified that the condensation route was the likely path for this nano MgO-Ag(0) catalyzed hydrogenation of 4-NTP. The probable reaction mechanism was shown in **Fig.11**.

Fig. 11

Conclusions:

In summary, a facile method for in-situ synthesis of nano MgO-Ag(0) hybrid nanomaterials with dispersive Ag NPs on the surface of nano MgO via Sn^{2+} linkage and reduction was developed. The diameter of the Ag NPs was 9.97±1.95 nm. Benefit from the synergy effect of nano MgO and Ag NPs, the nano MgO-Ag(0) exhibited excellent SERS and catalytical activities. The obtained nano MgO-Ag(0) nanocomposites were employed for the real time SERS monitoring of the reaction of 4-NTP to 4-ATP in aqueous medium. The intrinsic reaction kinetics and probable reaction mechanism of this reaction was also investigated. The catalytic reaction rate constant k was 0.0095 s^{-1} at room temperature, which was higher than that reported catalysts for the same catalytic reaction[15, 31, 32]. This SERS-based synergy technique provides a novel approach for quantitatively studying catalytic chemical reaction process, reaction mechanism and rate constants in similar experiments.

Acknowledgements

The work was supported by the National Natural Science Foundation of China (Nos.21277176, 21127008 and 21475153), the Major National Scientific Instrument and Equipment Development Project (No.2011YQ03012409), and the Guangdong Provincial Natural Science Foundation of China (Nos.S2013010012091 and 2015A030311020), respectively.

References

1 S. T. Daniells, A. R. Overweg, M. Makkee and J. A. Moulijn, *J. Catal.*, 2005, **230**, 52-65.

2 G. Richner, J. A. van Bokhoven, Y. M. Neuhold, M. Makosch and K. Hungerbuhler, *Phys. Chem. Chem. Phys.*, 2011, **13**, 12463-12471.

3 K. Shimizu, Y. Miyamoto, T. Kawasaki, T. Tanji, Y. Tai and A. Satsuma, *J. Phys. Chem. C*, 2009, **113**, 17803-17810.

4 B. Chowdhury, J. J. Bravo-Suarez, N. Mimura, J. Q. Lu, Kyoko K. Bando, S. Tsubota and M. Haruta, *J. Phys. Chem. B* , 2006, **110**, 22995-22999.

5 S. Nie and S. R. Emory, *Science*, 1997, **275**, 1102-1106.

6 K. Kneipp, Y. Wang, H. Kneipp, L. T. Perelman, I. Itzkan, R. R. Dasari and M. S. Feld, *Phys. Rev. Lett.*, 1997, **78** 1667-1670.

7 E. Cortes, P. G. Etchegoin, E. C. Le Ru, A. Fainstein, M. E. Vela and R. C. Salvarezza, *J. Am. Chem. Soc.*, 2010, **132**, 18034-18037.

8 K. N. Heck, B. G. Janesko, G. E. Scuseria, N. J. Halas and M. S. Wong, *J. Am. Chem. Soc.*, 2008, **130**, 16592-16600.

9 J. Huang, Y. Zhu, M. Lin, Q. Wang, L. Zhao, Y. Yang, K. X. Yao and Y. Han, *J. Am. Chem. Soc.*, 2013, **135**, 8552-8561.

10 W. Xie, C. Herrmann, K. Kompe, M. Haase and S. Schlucker, *J. Am. Chem. Soc.*, 2011, **133**, 19302-19305.

11 W. Xie, B. Walkenfort and S. Schlucker, *J. Am. Chem. Soc.*, 2013, **135**, 1657-1660.

12 R. Liu, J. F. Liu, Z. M. Zhang, L. Q. Zhang, J. F. Sun, M. T. Sun and G. B. Jiang, *J. Phys. Chem. Lett.*, 2014, **5**, 969-975.

13 M. Muniz-Miranda, *Appl. Catal. B-Environ.*, 2014, **146**, 147-150.

14 Z. Y. Bao, D. Y. Lei, R. Jiang, X. Liu, J. Dai, J. Wang, H. L. Chan and Y. H. Tsang, *Nanoscale*, 2014, **6**, 9063-9070.
15 W. Y. Cai, X. H. Tang, B. Sun and L. B. Yang, *Nanoscale*, 2014, **6**, 7954-7958.
16 X. H. Tang, W. Y. Cai, L. B. Yang and J. H. Liu, *Nanoscale*, 2014, **6**, 8612-8616.
17 X. F. Lang, T. T. You, P. G. Yin, E. Z. Tan, Y. Zhang, Y. F. Huang, H. P. Zhu, B. Ren and L. Guo, *Phys. Chem. Chem. Phys.*, 2013, **15**, 19337-19342.
18 X. Q. Ren, E. Z. Tan, X. F. Lang, T. T. You, L. Jiang, H. Y. Zhang, P. G. Yin and L. Guo, *Phys. Chem. Chem. Phys.*, 2013, **15**, 14196-14201.
19 B. Hvolbæk, T. V.W. Janssens, B. S. Clausen, H. Falsig, C. H. Christensenc and J. K. Nørskov, *Nano Today*, 2007, **2**, 14-18.
20 J. T. Krug, G. D. Wang, E. Sr and S. M. Nie, *J. Am. Chem. Soc.*, 1999, **121**, 9208-9214.
21 P. Jeevanandam and K. J. Klabunde, *Langmuir*, 2002, **18**, 5309-5313.
22 K. Layek, M. L. Kantam, M. Shirai, D. Nishio-Hamane, T. Sasaki and H. Maheswaran, *Green Chem.*, 2012, **14**, 3164.
23 K. Layek, R. Chakravarti, M. Lakshmi Kantam, H. Maheswaran and A. Vinu, *Green Chem.*, 2011, **13**, 2878.
24 J. Zheng, Y. Dong, W. Wang, Y. Ma, J. Hu and X. Chen, *Nanoscale*, 2013, **5**, 4894-4901.
25 W. Song, Y. X. Wang and B. Zhao, *J. Phys. Chem. C*, 2007, **111**, 12786-12791.
26 K. Zhu, J. Hu, C. Kübel and R. Richards, *Angew. Chem.*, 2006, **118**, 7435-7439.
27 R. M. Narske, K. J. Klabunde and S. Fultz, *Langmuir*, 2002, **18**, 4819-4825.
28 D. Y. Wu, L. B. Zhao, X. M. Liu, R. Huang, Y. F. Huang, B. Ren and Z. Q. Tian, *Chem. Commun.*, 2011, **47**, 2520-2522.
29 Y. F. Huang, H. P. Zhu, G. K. Liu, D. Y. Wu, B. Ren and Z. Q. Tian, *J. Am. Chem. Soc.*, 2010, **132**, 9244-9246.
30 B. Dong, Y. Fang, X. Chen, H. Xu and M. Sun, *Langmuir*, 2011, **27**, 10677-10682.
31 Y. W. Zhang, S. Liu, W. B. Lu, L. Wang, J. Q. Tian and X. P. Sun, *Catal. Sci. Technol.*, 2011, **1**, 1142-1144.
32 Z. Y. Bao, D. Y. Lei, R. B. Jiang, X. Liu, J. Y. Dai, J. F. Wang, H. L. Chan and Y. H. Tsang, *Nanoscale*, 2014, **6**, 9063-9070.
33 H. F. Gradual, *Z. Elektrochem.*, 1898, **4**, 506-513.

Figure captions:

Fig. 1 Schematic illustration of the preparation of nano MgO-Ag(0)

For the sake of convenience, interaction of only a part of O^{2-} ion with Sn^{2+} are shown.

Fig. 2 XRD pattern of (a) nano MgO-Ag(0) and (b) nano MgO

The figures in parentheses show the diffraction from planes corresponding to hydrated hexagonal crystalline phases of nano MgO. The red font indicate the planes corresponding to cubic crystalline phases of Ag(0) nanoparticles (a) and the blue font indicate the planes corresponding to cubic crystalline phases of nano MgO (b).

Fig. 3 (A) TEM images of the nano MgO-Ag(0), and (B) SAED pattern recorded from the silver nanoparticles of the nano MgO-Ag(0)

Fig. 4 (A) Survey spectra XPS of nano MgO-Ag(0), (B) Ag 3d XPS spectra of nano MgO-Ag(0)

Fig. 5 The SERS spectra of dye molecules and nucleobases used nano MgO-Ag(0) as SERS active substrate. The concentration of the dyes and nucleobases is 10 μmol L^{-1} and 50 μmol L^{-1}, respectively.

Fig. 6 The reproducibility of the as-synthesized nano MgO-Ag(0) substrate within (A) the same and (B) between different batches.

Fig. 7 Raw SERS spectra recorded during the nano MgO-Ag(0) catalyzed hydrogenation of 4-NTP using different volume of the reducing reagent $NaBH_4$. From top to bottom: the volume of $NaBH_4$ (100 mmol L^{-1}) solution is 0, 0.01 and 0.1 mL.

Fig. 8 Raw SERS spectra recorded during the nano MgO-Ag(0) catalyzed hydrogenation of 4-NTP with different reaction time.

Fig. 9 The SERS of the reaction product of 4-NTP and $NaBH_4$ used nano MgO (a and b), nano MgO-Ag(0) (c and d) and Ag NPs (e and f) as catalyst. The reaction time is 0 min (a, c and e). The reaction time is 10 min (b, d and f).

Fig. 10 plot of ln ($[I_{1347}]_0/[I_{1347}]_t$) versus time for the reduction of 4-NTP with nano MgO-Ag(0) as catalysts

Fig. 11 Probable reaction mechanism for the reduction of 4-NTP by $NaBH_4$ with nano MgO-Ag(0) as catalyst

Fig. 1

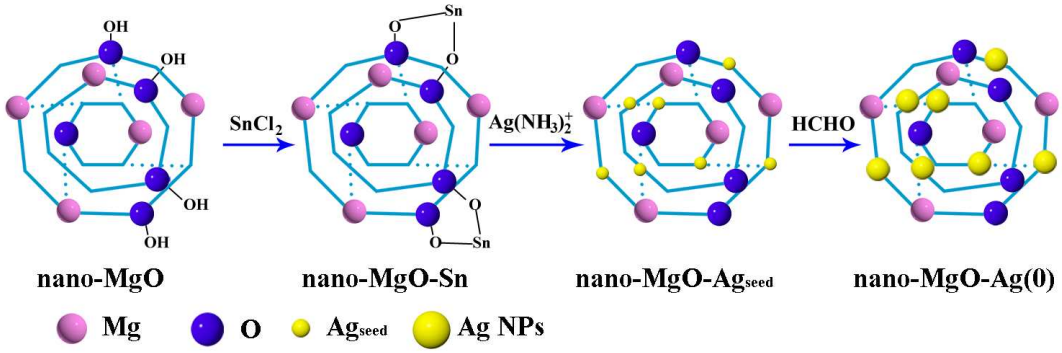

Fig. 2

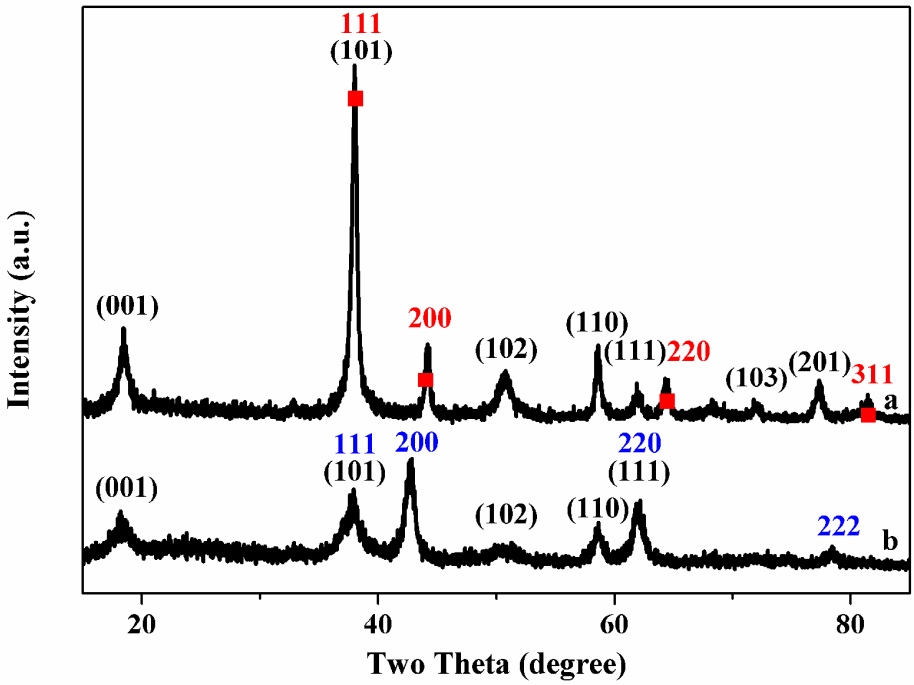

Fig. 3

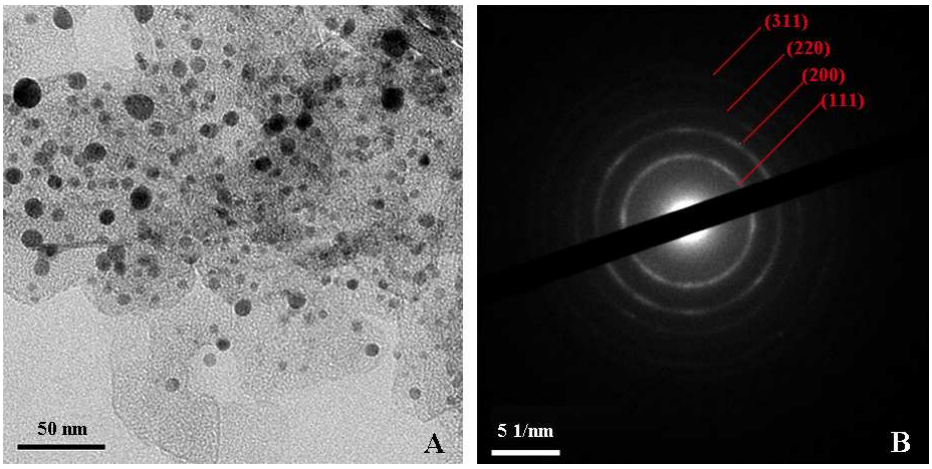

Fig. 4

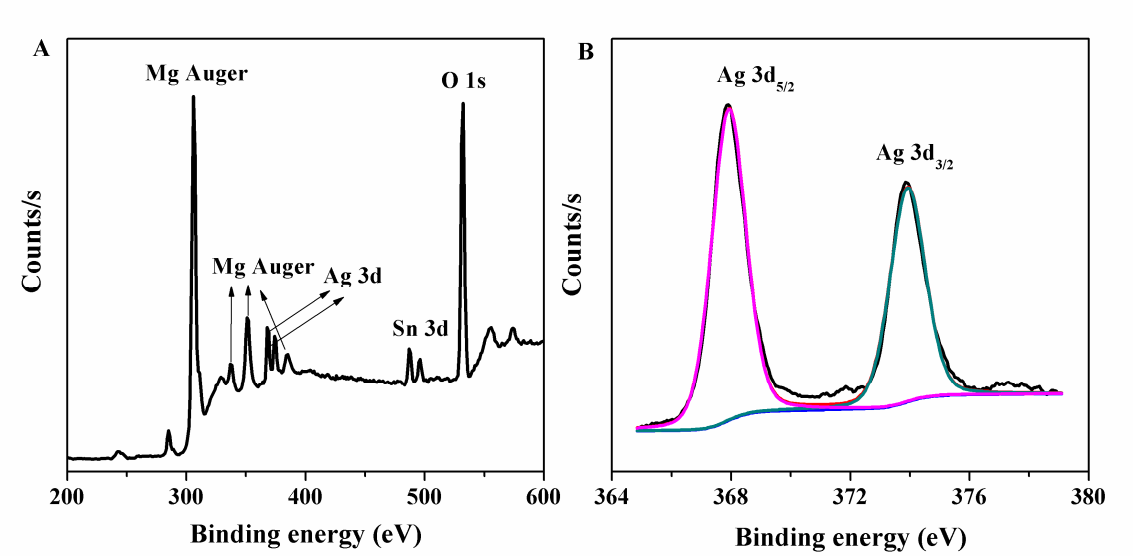

Fig. 5

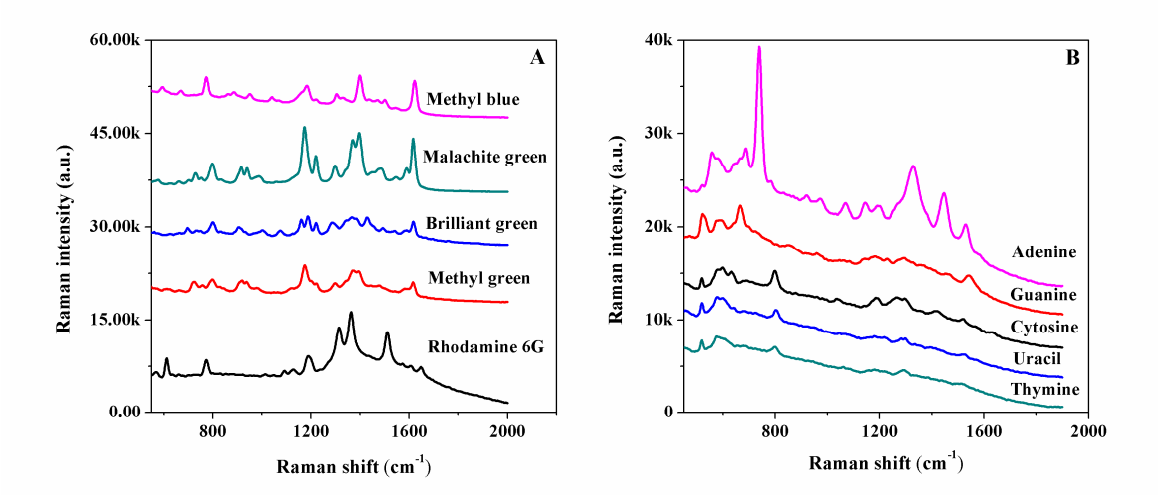

Fig. 6

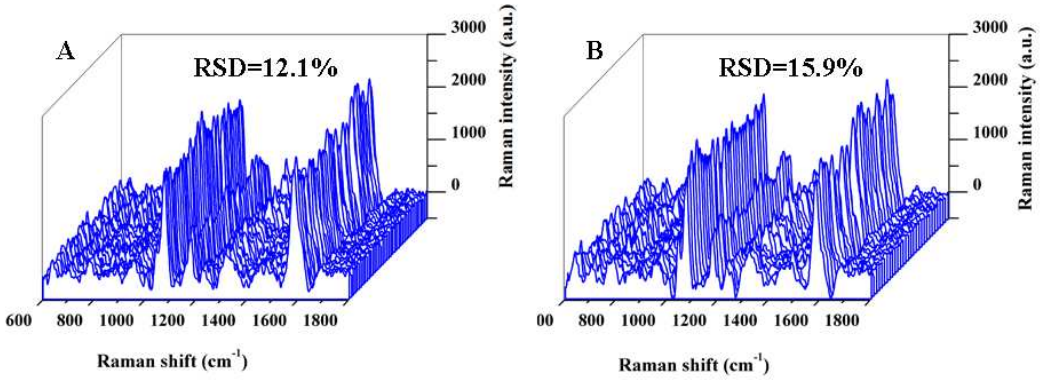

Fig. 7

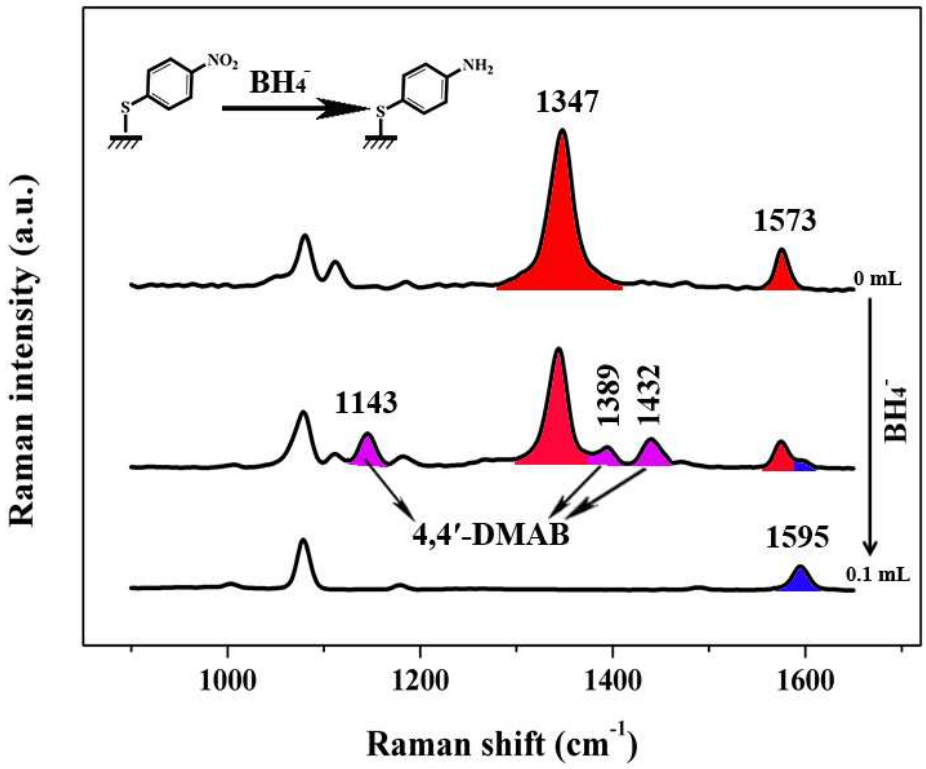

Fig. 8

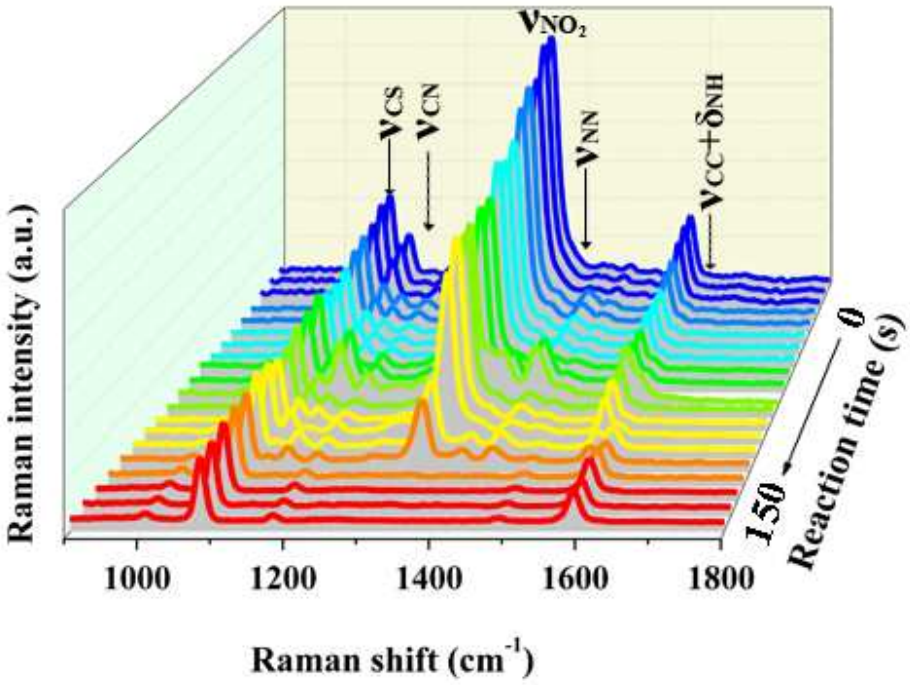

Fig. 9

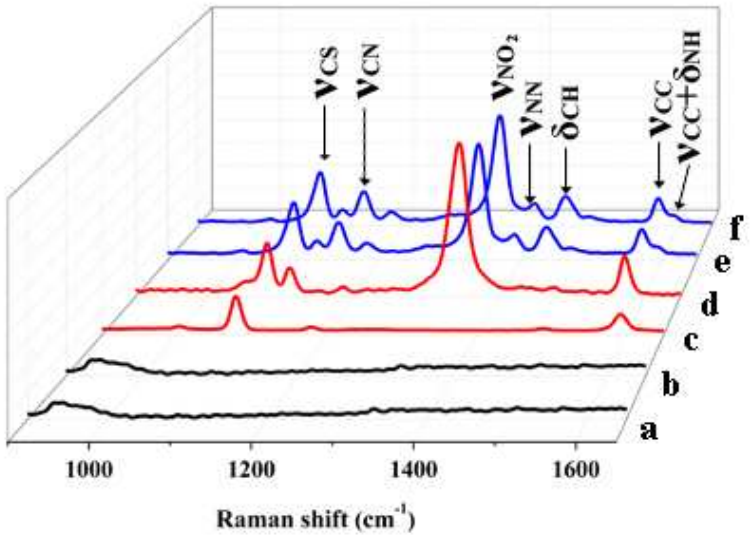

Fig. 10

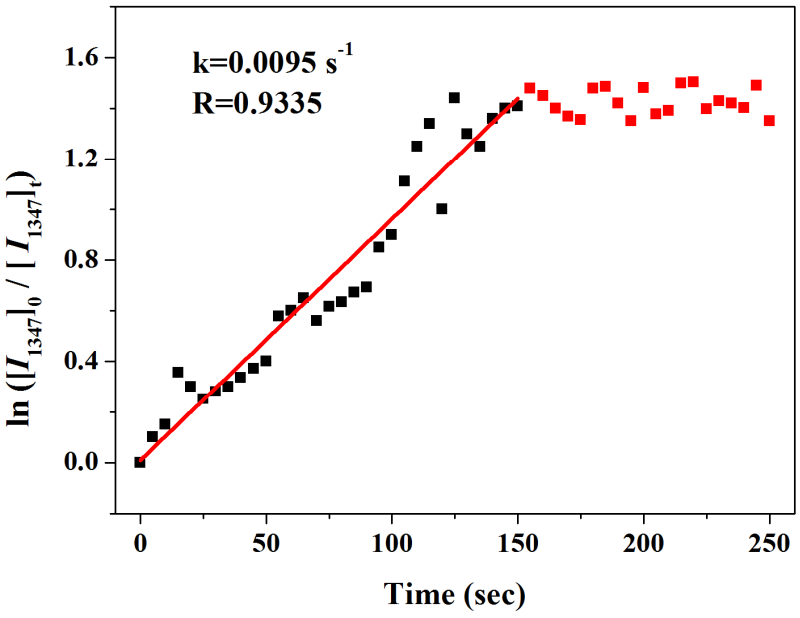

Fig. 11